Nonequilibrium self-assembly of metals on diblock copolymer templates

W. A. Lopes*
The James Franck Institute and Department of Physics, The University of Chicago, Chicago, Illinois 60637
(Received 2 March 2001; revised manuscript received 14 December 2001; published 21 February 2002)

Most studies of self-assembled systems reveal that the highest order is associated with equilibrium states of the system. By systematically studying metal decoration of diblock copolymer templates, I show that a high degree of order can arise under strongly nonequilibrium conditions. Under a wide range of conditions, thermally evaporated gold decorates ultrathin, asymmetric, polystyrene-*b*-polymethylmethacrylate diblock copolymer films with isolated nanoparticles. These particles aggregate into nanoparticle chains inside the polystyrene block with a selectivity approaching 100%. However, even at metal loading fractions of up to 30% by volume no coalescence into continuous nanowires is observed. This behavior is also shared by indium, tin, lead, bismuth, and silver at low coverage (<30 Å nominal thickness). At high coverage (>100 Å nominal thickness), however, silver self-assembles to form nanowires. One can understand the formation of the chains of nanoparticles by understanding the equilibrium state of the system (metal+polymer). The silver nanowires are highly nonequilibrium structures and, to the best of my knowledge, unexplained by existing theoretical models. Assuming an energy difference for metallic particles for either side of the diblock, a mobility difference, and an attractive interaction between metallic particles, I modeled the self-assembly of the nanowires with a Monte Carlo simulation. This Monte Carlo simulation qualitatively agrees with the formation of the silver nanowires and their relaxation to equilibrium upon moderate heating.

DOI: 10.1103/PhysRevE.65.031606 PACS number(s): 83.80.Uv, 81.07.−b, 81.16.Dn, 81.16.Rf

I. INTRODUCTION

Typically, the most perfectly ordered, self-assembled structures correspond to equilibrium states of the system. Examples abound in the literature on self-assembled colloidal crystals [1–4], nanocrystal superlattices [5], copolymer systems [6,7], metal wire formation on stepped crystal surfaces [8–16], and many others. Nonequilibrium growth or self-assembly modes, by contrast, are usually associated with structural disorder.

Here, I show that a high degree of order can arise out of strong nonequilibrium conditions. I consider the diffusion of metal on a patterned surface with a regular modulation of the surface properties on the scale of nanometers. My experiments focus on patterns produced by the phase separation of diblock copolymers. Similar to step edges on miscut crystal surfaces, ultrathin diblock copolymer films from parallel ''stripe'' domains that produce differences in the metal's ability to diffuse along or across the stripes. However, very much unlike wire formation along step edges, I find a rich set of highly ordered, yet out-of-equilibrium configurations for the metal that are not reflected in the equilibrium structure of the metal-on-polymer system. These include dense ''nanochains'' of metal nanoparticles selectively aggregated with near 100% selectivity in one of the copolymer domains as well as an experimental realization of continuous nanowires self-assembled on a diblock copolymer template. Remarkably, these nanowires are only stable under nonequilibrium conditions.

*Present address: Arryx Inc., 316 N. Michigan Ave., Suite CL 20, Chicago, IL 60601; email address: wlopes@arryx.com

Diblock copolymers naturally form patterns with length scales on the order of 10's to 100's of nanometers [6,7]. Further, diblock patterns can be selectively decorated both chemically [17–24] and physically [25–27], making diblocks an ideal system to study the self-assembly of nanostructures on structured substrates. The patterns in diblock copolymers flow from an interplay between energy and entropy. Diblock copolymers are polymers formed by joining two chemically distinct polymers (or blocks) end-to-end with a covalent bond. Since chemically distinct polymers tend to be immiscible, a large collection of such polymers will phase separate; but, because of the covalent bond, the polymers will only phase separate on length scales given by the polymer itself. In bulk, diblock copolymers self-assemble into regular arrays of lamellas, cylinders, or spheres [6,7].

To date, all methods for selectively decorating one block of a diblock with metals or insulators have resulted in well-isolated nanoparticles decorating one block of the diblock. Methods to arrive at extended, continuous arrays of metallic or semiconducting objects using diblock patterns as a template have required removing one of the blocks and using the film as a mask for plating [28,29] or etching through the film to transfer the pattern to a substrate [30–32]. There has been little research to delineate why all previous methods of decorating diblocks (with both blocks present) have resulted in arrays of nanoparticles instead of arrays of extended, continuous objects like wires.

In addition to the technological and scientific aspects of creating nanostructures, diblock films in their own right are good systems in which to study nonequilibrium phenomena. Diblock films confined between two rigid plates exhibit frustration [33–36]. Further, unconfined ultrathin films exhibit long-lived, metastable morphologies not found in bulk [37,38]. Diblock films in which a small fraction of monomers are quenched to stay on the substrate are expected to

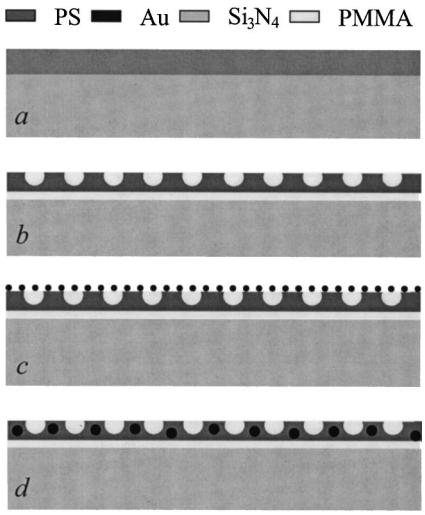

FIG. 1. Sketch of fabrication process. (a) Spin coat Si_3N_4 substrate with ~2% solution of diblock in toluene. (b) First anneal, microphase separate diblock film in ~250 °C oven with Ar atmosphere. (c) Evaporate metal onto diblock template. (d) Second anneal, improve metal selectivity and diffuse metal into diblock film by annealing in Ar atmosphere.

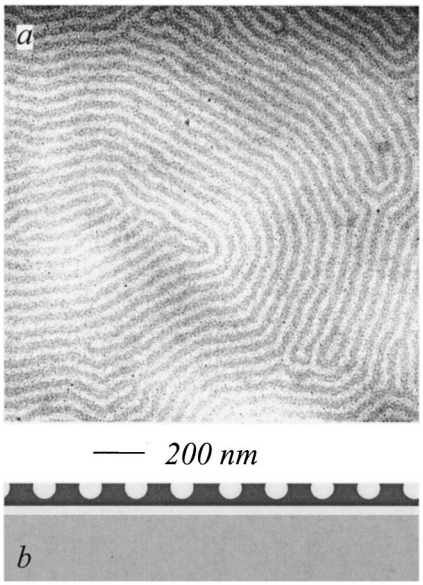

FIG. 2. Ultrathin film of PS-*b*-PMMA diblock copolymer. (a) TEM (top view). Light lines in the micrograph correspond to the PMMA-rich regions of the film. Dark lines correspond to the PS-rich regions of the film. The scale bar in the figure is 200 nm long. (b) Sketch of cross section of diblock film (based on results from Morkved, Ref. [38]).

alter their orientation from that of equilibrium films [39]. Recently, diblock films have been studied with atomic force microscopy (AFM) to study the motion of defects as the films approach equilibrium [40,41].

In this paper, I report on a systematic study of metalic decoration of diblock copolymer ultrathin films. I take the diblock template and its morphology as given and focus on the aggregation of evaporated metal onto the template. I organized this paper as follows. After describing the details of sample fabrication and characterization (Sec. II), I describe experimental results in Sec. III. I observe two distinct behaviors for selectively decorating the diblock copolymer: either the metal decorates the diblock copolymer template with nanoparticles or the metal decorates the template with nanowires [42]. I focus on the results obtained with gold and silver on polystyrene-*b*-polymethylmethacrylate diblock (PS-*b*-PMMA)—gold forms nanochains and silver forms nanowires. In the discussion section (Sec. IV), I find that the case of nanoparticles can be understood by examining the equilibrium state of the (metal+polymer) system. However, the case of nanowires requires an understanding of the nonequilibrium processes that build the wires. To study these processes, I modeled the formation of the nanowires with a two-dimensional (2D) Monte Carlo simulation.

II. EXPERIMENTAL DETAILS AND PROCEDURE

Fabrication of my samples followed a four-step process as sketched in Fig. 1. The process starts by spin coating an ultrathin film of diblock copolymer from solution onto a substrate [Fig. 1(a)]. During the first annealing step, the diblock phase separates. This produces a fingerprintlike pattern in which both blocks alternate along the film surface [38] and form a template for the further self-assembly of metal [25] [Figs. 1(b) and 2]. Decoration of the film is achieved by evaporating a small amount of metal (nominal thickness 5 to 120 Å) onto the surface of the diblock film [Fig. 1(c)]. Optionally, one completes creating the samples by annealing the sample for a second time in an argon atmosphere.

As substrates, I chose the free standing, amorphous Si_3N_4 membranes described by Morkved *et al.* [43] The advantage of these substrates is that they allow for investigation of samples by both transmission electron microscopy (TEM) and AFM without further sample processing.

The copolymer used in the experiments described here was asymmetric PS-*b*-PMMA diblock (Polysciences Inc.) with a molecular weight of 84 000 (PS $M_w=60\,000$; PMMA $M_w=24\,000$) and polydispersity of 1.08. In bulk, this diblock forms parallel cylindrical domains with a repeat spacing of 50 nm. I Soxhelt extracted the diblock with cyclohexane to remove any excess homopolymer PS. The solution I used for spin casting was, nominally, 2.3% by weight diblock in toluene. I chose a spin speed such that, after the first anneal, the thickness of the polymer film was equal to the repeat spacing of the diblock; typically, I cast my films at a speed between 3000 and 4000 rpm for 1 min.

I used a 100% argon atmosphere during all annealing steps to avoid oxidation of the samples. Both annealing cycles followed the same sequence: a ramp at 5° per min to a maximum temperature $T_{\max}$ followed by a waiting time t_w, at $T_{\max}$ and, finally, a ramp back down to room temperature at approximately $-2°$ per min. For the rest of this paper I will report only $T_{\max}$ and t_w. Typical conditions for the first anneal were $T_{\max}=290\,°\mathrm{C}$ and $t_w=1$ min. Longer annealing times t_w did not damage the film; rather, they decreased the number of defects in the fingerprint pattern, in accord with previous results by Hahm *et al.* [40] and Harrison *et al.* [41].

Further, the decoration results reported in this paper are identical to the results obtained on diblock samples annealed at $T_{max}=165\,^{\circ}C$ for $t_w=3$ days; thus, thermal damage to the diblock film is not responsible for my results. Figure 2(a) shows a TEM micrograph (overview) of a typical diblock film prepared in this manner. PMMA domains of the film appear lighter due to electron beam thinning of the PMMA [44]. The morphology of phase-separated films consists of half cylinders of PMMA surrounded by a PS matrix with both blocks present at the surface of the diblock film [38]. A sketch of this morphology, based on Ref. [38], is presented in Fig. 2(b).

During the evaporation step, I heated a tungsten boat containing the metals to temperatures such that the metals (gold, silver, etc.) evaporated from the source at a constant rate between 0.1 to 0.2 Å per second as measured with a quartz crystal monitor. The background pressure for the evaporation chamber was 1×10^{-6} Torr. For the results reported here, all evaporations were performed at room temperature. Evaporation leaves most of the metal at the polymer film/air interface and scattered over the surface as sketched in Fig. 1(c). T_{max} for the second anneal did not exceed 250 °C and t_w for the second anneal was chosen to maximize either the density of nanoparticles in the decorated pattern or the selectivity of nanoparticles within the template. In all cases, t_w did not exceed 12 h.

I investigated my samples with TEM and AFM. TEM micrographs were taken with a Phillips CM120 transmission electron microscope operating at 120 kV. AFM micrographs were taken with a digital instruments multimode atomic force microscope operating in tapping mode.

III. EXPERIMENTAL RESULTS

I obtained results on six metals (gold, silver, indium, lead, tin, and bismuth) that decorate the diblock template selectively. With the exception of silver, all of these elements self-assemble into nanoparticles distributed inside one of the blocks. In the following, these structures will be called ''nanochains.'' Only silver was found to form continuous nanowires at high coverage (>100 Å). Moderate heating brings the wires closer to equilibrium and destroys them. In this section, I will describe these findings in more detail. Since gold, indium, lead, tin, and bismuth showed similar behavior, in Sec. III A, I will focus results from decorating the diblock templates with gold to describe the nanochains. Which block the metals decorate is element dependent. Indium, tin, lead, and bismuth decorate the PMMA, while gold and silver decorate the PS. In Sec. III B, I will describe the arrays of silver nanowires and their relaxation to equilibrium. And finally, in Sec. III C, I will describe evaporation of silver onto PS and onto PMMA homopolymer films as a way to investigate how silver behaves in each domain of the diblock template.

A. Selective decoration I: Nanochains

Figure 3 shows typical TEM results from gold decoration. Electrons scatter much more strongly from the gold than from the organic polymers and I identify the dark gray and black shapes in the micrographs with gold nanoparticles. Figure 3(a) shows a section of a sample after evaporating 30 Å of gold onto the diblock template but before the second anneal. Already, selective aggregation is apparent. Annealing the sample to 180 °C for 1 min increases the selectivity of the decorated pattern dramatically [Fig. 3(b)]. By repeating this experiment with only 5 Å of evaporated gold on the template, I can identify contrast from the diblock and conclude that the gold preferentially decorates the PS domains that appear dark in TEM [45]. Annealing the 30 Å samples at 180 °C for 6 h agglomerates the gold into larger (~25 nm) nanoparticles inside the PS domains. This increases the spacing between the nanoparticles, but leads to a selectivity of ~100% [Fig. 3(c)]. As Lin *et al.* showed in the case of gold on polystyrene-*b*-poly(2-vinylpyridine) (PS-PVP) [46], I expect nanoparticles to diffuse also into the diblock film during the second anneal [see Fig. 1(d)]. In order to increase the density of gold nanoparticles in the PS domains, I repeated

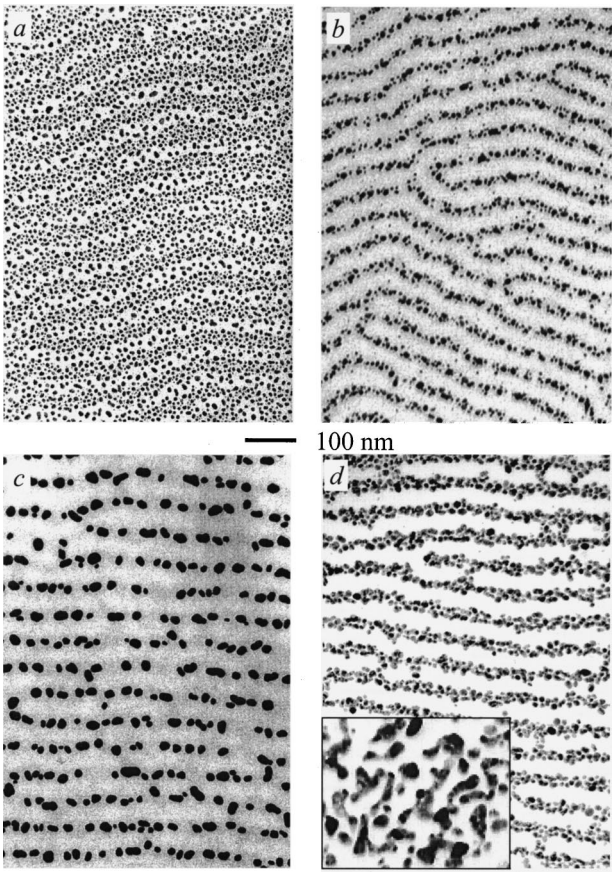

FIG. 3. Selective gold decoration of PS-*b*-PMMA. Gold scatters electrons more efficiently than the organic polymers and appears dark gray or black in these TEM micrographs. Scale bar is 100 nm long. (a) TEM of 30 Å gold on diblock film as evaporated. (b) TEM of similar film after second anneal at 180 °C for 1 min. (c) TEM of similar film after second anneal to 180 °C for 6 h. (d) TEM of film after six repeated evaporation and anneal steps of 10 Å gold and anneal to 180 °C for 1 min. Inset to (d) TEM of film where I evaporated 60 Å gold in one step. The inset has the same size scale as the other parts in this figure.

the evaporation and second annealing steps under conditions identical to the ones that lead to Fig. 3(b) ($T_{max}=180\,^{\circ}C$, $t_w=1$ min). Repeating this procedure with six evaporations of 10 Å of gold each leads to a high density of nanoparticles inside the PS domains [Fig. 3(d)]. For this particular sample, the gold occupies approximately 30% of the volume of the PS domain. At this degree of metal loading, the metallic particles are close enough to support a tunneling current and the samples display highly nonlinear current-voltage characteristics [47].

During the evaporation step, atomic gold diffuses on the substrate and agglomerates to form nanoparticles. These nanoparticles increase their size by either capturing more atomic gold or by agglomerating with other nanoparticles. I found that the above decoration results hold, in general, so long as during the evaporation step the gold particles do not connect across the PMMA domains to form a bridge connecting gold particles in the adjacent PS domains. For gold evaporated at 0.1 Å/s, this limit happens around a nominal thickness of 60 Å. After that point, gold nanostructures ignore the domain pattern and no amount of annealing returns the sample to a state where the gold follows the template. An example of this effect is shown in the inset to Fig. 3(d).

While the results shown in Fig. 3 were obtained for gold, all metals that I observed to selectively decorate the PS-b-PMMA diblock exhibit the following generic behavior.

(1) The metals show some degree of selective decoration upon evaporation onto the template and before any subsequent (second) anneal.

(2) Annealing at temperatures above the diblock's glass temperature increases the selectivity of decoration. Higher selectivity is reached at higher temperatures.

(3) Above an element-dependent limiting thickness, the behavior of large metal nanoparticles appears to be dominated by interactions with other metallic nanoparticles rather than by the interaction with the diblock template.

For low coverage, silver decoration looks qualitatively similar to the gold case. Figure 4(a) shows a TEM image (before the second anneal) of a diblock template onto which I evaporated 25 Å of silver. The large swath in the picture where there is no silver (no black dots) corresponds to a section in the sample where the silver has been removed from the sample by a piece of dust that scratched the surface. This allows us to unambiguously identify that the silver is at the surface of the sample and that the silver decorates the PS domains. At low coverage (<30 Å), the most striking qualitative difference between this result and the gold case immediately after evaporation [Fig. 3(a)] is that the silver-decoration pattern already approaches 100% selectivity before the second anneal. Gold-decorated samples only reach 100% selectivity after the second anneal [Fig. 3(c)]. Further annealing of low coverage silver samples yield results qualitatively similar to long annealing times for gold [Fig. 3(c)].

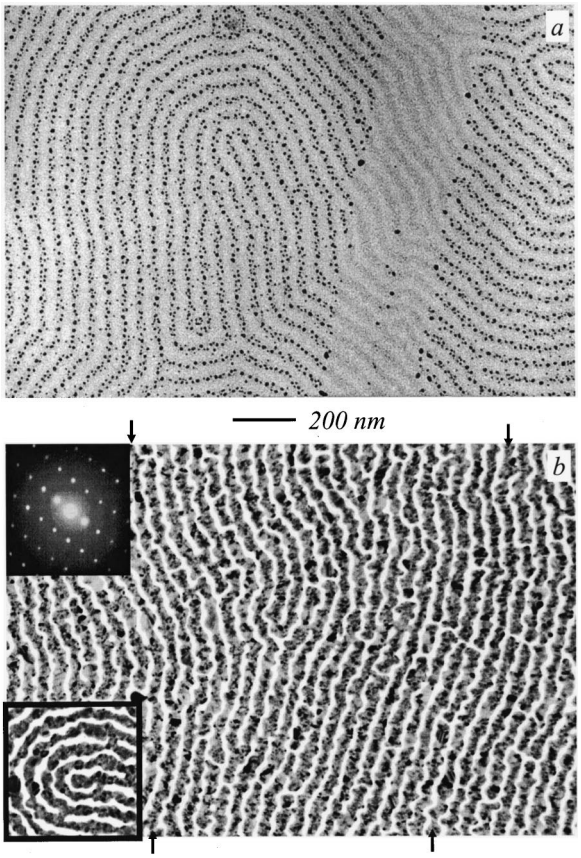

FIG. 4. Selective silver decoration of PS-*b*-PMMA. Silver appears dark in these TEM micrographs. Scale bar in figure is 200 nm long. (a) TEM of decoration pattern for 25 Å of evaporated silver. (b) TEM of decoration pattern for 120 Å of silver evaporated at 0.15 Å/s. Arrows point to wires that span the width of the figure. Insets to (b) upper, typical electron diffraction pattern from a single nanocrystallite. Lower, decoration pattern from evaporation of 110 Å silver at 0.8 Å/s.

B. Selective decoration II: Nanowires

Since the volume of metal that decorates a particular domain is proportional to the total amount of metal that has been evaporated onto the template, it is tempting to think that a sufficiently large amount of metal might coalesce individual particles into nanowires. For most elements, however, point (3) above, prevents wire formation. The first hint of different behavior occurs with silver at intermediate thickness of evaporated metal (nominally between 60 and 90 Å), silver clusters from elongated shapes that align themselves on the template along the PS domains. The average aspect ratio of these clusters increases with increasing coverage of evaporated metal. As such, the limiting thickness in behavior, [point (3) above], is significantly higher for silver than for other metals.

Figure 4(b) shows a TEM micrograph for a sample with 120 Å of silver deposited during one evaporation step and no further anneal. Several of these polycrystalline silver structures have grown to be microns in length. For instance, black arrows in Fig. 4(b) point to two such wires that span the width of the image. The differing gray levels in the figure are produced by diffraction effects due to the interaction of the electron beam with the silver crystal planes and reflect differences in the orientation of silver crystallites. The upper inset to Fig. 4(b) shows an electron diffraction pattern taken

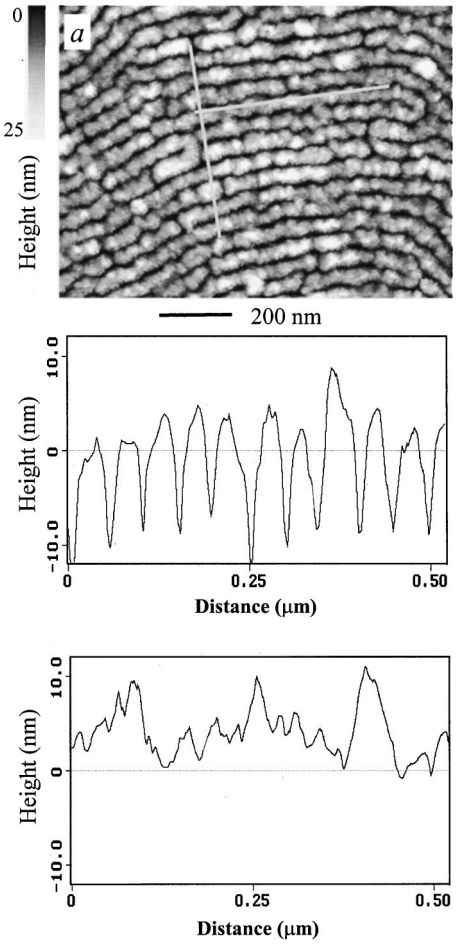

FIG. 5. Atomic force microscopy of 120 Å silver sample. (a) Micrograph of silver nanowires. Gray level in the micrograph ranges from 0 to 25 nm (white is the highest). Black lines in figure correspond to places where the cross sections in parts (b) and (c) were taken. Scale bar is 200 nm long. (b) Cross section of (a) taken perpendicularly to the nanowires. (c) Cross section of (a) taken parallel to the nanowires.

from one of the silver crystallites. The Si_3N_4 substrates are amorphous, do not produce such diffraction patterns on their own, and contribute only a uniform background scattering. The rate at which silver is deposited onto the template does not have a large impact on the wire formation. The lower inset to Fig. 4(b) is a TEM micrograph taken from a sample where the silver was evaporated at a rate of 0.8 Å/s, five times the evaporation rate for the sample shown in the main panel. This micrograph looks qualitatively identical to the sample decorated at the lower evaporation rate.

Since TEM projects three-dimensional density information onto a two-dimensional plane, it is not clear from these micrographs whether overlapping silver nanoparticles distributed throughout the thickness of the film form the wirelike structures or whether the structures are indeed contiguous along the film surface. Figure 5 attempts to resolve this question with AFM. Figure 5(a) displays the topography signal from a sample in which 120 Å of silver has been evaporated on to the diblock template. The various gray levels in

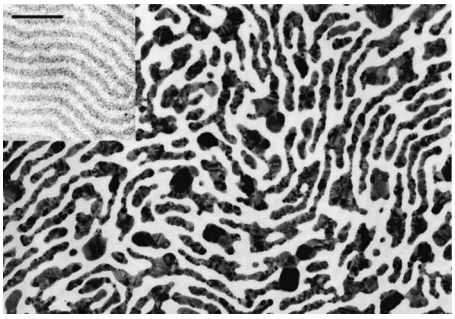

FIG. 6. TEM of 120 Å silver sample after second anneal ($T_{max}=90\,°C, t_w=3$ h). Scale bar is 200 nm long. Inset, TEM of similar sample after removal of silver with gold etch.

the picture span 25 nm. [The silver structures, which appear light in the image, appear wider in Fig. 5(a) than in Fig. 4(b) due to convolution with the AFM tip.] The lines drawn on the topograph correspond to cross sections of the data shown in Figs. 5(b) and 5(c). The corrugation amplitude of 10 to 18 nm is an order of magnitude larger than the corrugation present on the blank diblock template [40,43] and is consistent with all the evaporated silver sticking to the surface and agglomerating on the PS domains. As shown in Fig. 5(c) the roughness along the stripes is not as large until the cross section happens to step off the silver structure. Figure 5 thus indicates that the silver on the diblock is arranged in contiguous *silver nanowires*.

Next, I turn to the question of whether or not the wires correspond to equilibrium structures. Figure 6 shows a sample created identically to the samples in Figs. 4 and 5, after it had been subjected to a second anneal of 90 °C for 3 h. As is clear from the figure, most of the wirelike structures have broken apart and have started to ''ball up.'' Many of the larger silver structures have the same gray level throughout much of their mass, indicating that they have the same crystal orientation. Control samples created during the same run but not subjected to the second anneal remained identical to the samples shown in Figs. 4 and 5. The nanowires represent extremely long-lived states: TEM micrographs of silver wires nine months old and without a second anneal look qualitatively indistinguishable from the data presented in Figs. 4 and 5. Note that the important equilibrium temperatures for the system are the glass temperature of the diblock (between 100 and 105 °C [48]) and the melting temperature of the silver. The melting temperature for an 8 nm diameter silver crystal is approximately 470 °C and entities with larger diameters are expected to melt at higher temperatures [49]. Since the nanowires and their underlying templates were heated to a temperature below either of these values and the structures changed significantly, it is clear that the nanowires were in a nonequilibrium state.

To rule out that the diblock was involved in the relaxation of the silver wire structures, I used a buffered gold etch to remove the silver from a sample identical to that shown in Fig. 6. A TEM micrograph from the etched sample is shown in the inset to Fig. 6. The diblock template is obviously unaffected by the wire's formation and subsequent relaxation.

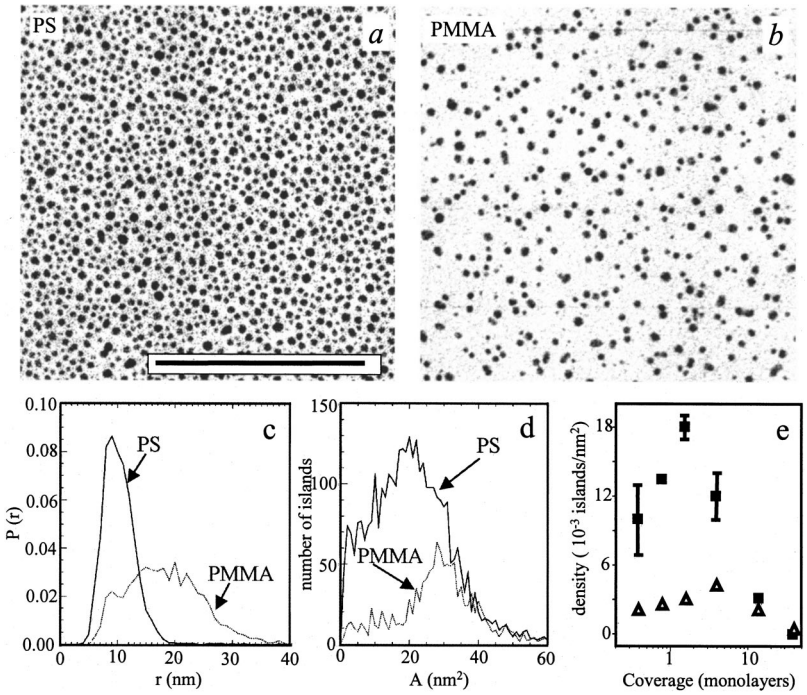

FIG. 7. Silver evaporated onto PS and PMMA homopolymer. Scale bar is 200 nm long. (a) TEM of 10 Å of silver evaporated onto PS. (b) TEM of 10 Å of silver evaporated onto PMMA. (c) Distribution of nearest neighbor distances (center-to-center distance). (d) Histogram of nanocluster areas. (e) Number density of nanoclusters vs total amount of silver evaporated. Filled square symbols (■) are data points for PS samples. Triangle symbols (△) are data points for PMMA samples. I did not plot error bars when the bars were smaller than the corresponding data points.

C. Comparison with isotropic substrates: Decoration of homopolymers

To find out how the behavior of the silver depends upon which domain of the diblock template the silver lands, I evaporated silver onto homopolymer PS and PMMA. I chose the molecular weight of the homopolymers to be identical to the molecular weight of individual blocks that make up the diblock. Figures 7(a) and 7(b) are TEM micrographs of representative samples of homopolymer PS and PMMA onto which I simultaneously evaporated 10 Å silver at 0.1 Å/s. Inspection of Figs. 7(a) and 7(b) indicates a much larger density of silver on the PS than on the PMMA sample. From counting the number of islands, I find that this effect exists for all coverages less than 11 monolayers [Fig. 7(c)]. (For larger coverages, continuous silver films form and formation of isolated islands ceases.)

Three possibilities could lead to this different behavior: the silver particles could be distributed throughout the thickness of the PMMA sample and some silver particles could be shadowing others, atomic silver could be much more likely to leave the surface of PMMA than PS, or the diffusion constant of silver could be higher on PMMA than on PS. Tilting the PMMA homopolymer samples in the microscope, for angles up to 45°, did not bring more particles into view and did not alter the shape of the particles in view in any statistically significant way. That is, the silver particles appear to be spherically shaped and do not shadow each other in the electron microscope. Under the assumptions that atoms are deposited on a surface at random, isolated atoms are mobile, there are no defects that would irreversibly trap atoms, growth of clusters of atoms happens in three dimensions, and the dynamics of assembly are not dominated by atoms leaving the surface of the substrate, Jensen and coworkers find [50] that the maximum density of particles on a two-dimensional substrate is inversely proportional to the diffusion constant to the power $\frac{2}{7}$. Further, PS provides no measurable defects for silver that would trap the silver atoms and inhibit diffusion and silver interacts more strongly with PS than with PMMA. Therefore, if the diffusion constant of silver is larger on PMMA than on PS, the peak of the nearest neighbor distribution should be at a larger distance for the PMMA samples than the PS samples. Also, assuming constant volumes of silver, the average area of the individual silver nanoclusters in the PMMA samples should be larger than in the PS samples. The peak of the nearest neighbor distribution is certainly at a larger distance for the PMMA sample as is confirmed in Fig. 7(c). As is evident from a histogram of the areas of the clusters in each sample [Fig. 7(d)], the average cluster size is larger for the PMMA sample than for the PS sample. What is also clear from the histogram, however, is that for each area measured, the number of clusters on the PS sample is greater than or equal to the number of clusters on the PMMA sample. Assuming that the particles are spheres, a simple consistency check reveals that, while the peak of the nearest neighbor distribution is consistent with the average area for silver clusters in the PS homopolymer samples, it is not consistent for the PMMA homopolymer samples. The volume of silver on the PMMA sample is less than the volume of silver on the PS sample. Silver must, then, leave the surface of the PMMA at a greater rate than the PS sample. Atoms of silver could leave the surface of the PMMA through any combination of three routes: they could simply be less likely to stick to the surface when they first hit it, they could diffuse into the bulk of the PMMA film, or atoms of silver could evaporate off the surface after they have diffused around for a while. The present study does not identify which, if any, of these effects is the dominant method for removing silver from the surface of the PMMA homopolymer, and for simplicity, I will refer to any effect that removes silver as ''evaporation.'' I conclude then

that the rates of diffusion and evaporation differ on the two homopolymers. Similar conclusions about the difference of diffusion and evaporation rates hold for samples where the total amount of silver deposited onto the samples ranges from 0.4 to 4 monolayers. Data for much higher coverage (approximately 14 monolayers or higher) are harder to interpret because the silver films become continuous.

IV. DISCUSSION AND MODEL

In the experimental section, I described two distinct observed behaviors: evaporated metals selectively decorate the diblock template but without ever forming wires, or, the evaporated metals selectively decorate the diblock template by forming wires. I will consider each of these behaviors in turn. With gold and the other metals, I will put my experimental results into the context of other studies of metal decoration of diblock copolymers and explain why repeated evaporation and anneal cycles is necessary to selectively decorate at high coverage. At high coverage, with the exception of silver, I never observed nanowires. Looking at the expected equilibrium behavior for these metals, I find a possible explanation. This explanation though, would also hold for silver. Then why does silver form nanowires? To the best of my knowledge, this behavior is not captured by any of the established theoretical approaches. However, a Monte Carlo simulation I developed can qualitatively reproduce the formation and eventual breakup of the silver nanowires. Section IV A will discuss the gold decoration results while Sec. IV B will present results from the simulation and relate them to the silver wire results.

A. Discussion of experimental results

At 1×10^{-6} Torr, the mean free path of atoms is much larger than the source-substrate distance in the evaporator used for sample preparation; therefore, one may assume that the evaporated metal arrives at the substrate in its atomic form. Upon arrival at the surface of the diblock film, metal atoms can do one of four things: bounce off the surface, diffuse around on the surface, diffuse into the film, or evaporate off the surface after some initial diffusion. The relative rates for these processes, together with the rate at which metal nanoparticles form by aggregation, determine the structure of the deposited metal film. Lin *et al.* performed x-ray reflection standing wave fluorescence spectroscopy in combination with x-ray reflectivity and grazing-incidence diffraction on gold-decorated PS-*b*-PVP diblocks both before and after the second anneal [46]. They fit the density profile of the as-evaporated gold to a Gaussian profile with a peak 4 nm below air interface. Their best-fit profile had a nonnegligible presence at the air interface and extended no more than 10 nm into the polymer film. After the second anneal of 150 °C for 12 h, their best-fit profile changed to one where the gold was practically nonexistent within 12 nm of the air interface, but uniformly distributed throughout most of the rest of the film. Assuming that the gold-decorated PS-*b*-PMMA films behave similarly, the gold in Fig. 3(a) is on top of the diblock film. Both the mean size of the gold nanoparticles and the average nearest neighbor distance are larger in the PMMA than in the PS, consistent with a larger diffusion constant for gold in PMMA than in PS. During the second anneal, in analogy with the work of Lin *et al.*, I expect that the gold diffuses into the diblock film and finds a place within the diblock that is energetically most favorable. From Fig. 3(c), the most favorable position is clearly within the PS-rich regions of the film. Such an energetic interaction would explain why, with low loading and long annealing times [Fig. 3(c)]. I never observe any gold nanoparticles in the PMMA domains.

The trick to decorating the diblock with a large amount of gold [$\geqslant$60 Å as in Fig. 3(d)] while retaining an ordered pattern, is to repeat a cycle of evaporating small amounts of gold and annealing the sample so that the gold diffuses away from the air interface. If all 60 Å were available at the surface, gold-gold interactions would overwhelm the gold-polymer interaction. The metal would, then, agglomerate and ignore the template as in the inset to Fig. 3(d). Consequently, one should be able to control the number of defects in the decoration of the 60 Å gold samples by increasing the number of evaporation and anneal cycles and by simultaneously reducing the amount of gold deposited during each evaporation step. Indeed, the number of defects in which two parallel lines of gold nanoparticles are joined by a bridgelike collection of gold nanoparticles depends on the amount of gold deposited during the repeated evaporation and anneal steps. Samples where the 60 Å of gold was evaporated in three 20 Å steps have many more bridges than samples where the 60 Å of gold was evaporated in six steps. Performing the evaporation on a stage heated to 150 °C and reducing the evaporation rate to 0.05 Å/s produced a sample with at most ten such bridges in a square micron area.

Consistent with the results in Fig. 3, I have never found preparation conditions for gold samples that lead to the formation of nanowires. One explanation for this behavior is that in their equilibrium state on the diblock template of the gold particles are spherical. The surface tension of gold is approximately 1.3 to 1.4 J/m^2 [51,52]. The surface tension of the polymers is approximately 3×10^{-3} to 4×10^{-3} J/m^2 [53]. From the measured interaction of benzene with gold as a function of distance [54], I estimate the interaction energy between PS and gold to be between 0.1 and 0.3 J/m^2. Thus, the gold particles will reach equilibrium by minimizing their surface area. The gold particles, then, stay close to their equilibrium state by staying in a spherical shape rather than forming long, wirelike structures. Given that the surface tension for silver is 1.2 to 1.4 J/m^2 [55,56], and the silver-silver interaction is known to dominate over the silver-PS interaction [57], one would expect that the equilibrium configuration for silver on the diblock template is also spherical. My experimental evidence corroborates this. From Figs. 4(a), 7(a), and 7(b), at low decoration, silver forms spheres on both the diblock and the homopolymers. Comparing Figs. 4(b) and 6, I also see that silver relaxes from the nonequilibrium nanowires into bulbous shapes that will further relax, presumably, to the equilibrium spherical shape. Then why does silver remain in the long lived (>nine months), nonequilibrium wire state?

As far as I know, there are no currently available theoretical models that answer this question. The models that I am aware of require an adhesive energy comparable to the cohesive energy of the metals that make the wires. For example, models of nanowire self-assembly on stepped, crystalline surfaces emphasize dangling chemical bonds or extra bonding partners at the step edges [14]. Viewing the step edge as merely a chemically distinct stripe and doing a direct comparison with the diblock template is misleading. In the diblock template, the domains extend for hundreds of atomic spacings, while, on the stepped templates, the step edges are localized to a width of approximately one atom. Studies of wirelike states of water condensed onto hydrophobic and hydrophilic striped substrates may be more closely related [58–60]. In this work, the substrate has been chemically patterned into neighboring stripes of the hydrophilic and hydrophobic surface characteristics. However, the resulting wirelike solutions are *equilibrium* states for the water. Further, water is pinned to the boundary between the hydrophilic and the hydrophobic regions by an abrupt change in the contact angle at the boundary. Given the very small magnitude of the surface energies of PS and PMMA in comparison to the surface energies of silver, silver's contact angle does not change significantly at the boundary between the PS and the PMMA domains in the copolymer template. Further, a comparison of Fig. 4(b) with Fig. 2(a) shows that silver is not pinned at the boundary between the two regions, because the edges of the silver wires do not reproduce the locally straight boundary between the PS and PMMA domains.

Before going into detail on the Monte Carlo simulations, I now summarize the central findings from my experiments of silver decoration of the diblock templates and of the homopolymer films. The following will serve as important benchmarks for the simulations to compare to.

(1) Silver lands on the polymer films in its atomic form and diffuses on the surface and sometimes evaporates from the surface.

(2) Both diffusion and evaporation rates occur at differing rates on the differing blocks of the diblock template (Fig. 7).

(3) The difference in evaporation rate from the differing blocks of the diblock template does not qualitatively affect nanowire formation. If it did, multiplying the flux of silver arriving at the template by a large factor would qualitatively change the nanowires formed; but changing the flux of silver by a factor of five does not have a pronounced effect on the nanowires [Fig. 4(b) and lower inset].

(4) When nanoclusters of silver join, they adhere to each other in differing crystal orientations [differing gray levels in Fig. 4(b)].

(5) The wires of Figs. 4 and 5 are not fractal objects and their surfaces are relatively smooth. This can be attributed to silver atoms diffusing along the surface of the silver structures.

(6) During the second anneal (Fig. 6), wires break, the resulting silver structures become more bulbous and ignore the template, and regions of constant crystalline orientation expand.

(7) The diblock template is unaffected by the creation of the wires or their relaxation during the second anneal (Fig. 6).

(8) The silver-silver interaction dominates the silver-polymer interaction [57].

B. Monte Carlo simulations

Kinetic Monte Carlo (KMC) simulations and methods from mean field theory have been used to successfully model thin film growth on homogeneous crystalline substrates [61–63], even achieving wirelike island shapes on surfaces with anisotropic diffusion constants or sticking coefficients that depend on direction [62,64–66]. Furthermore, KMC simulations have the advantage over traditional Monte Carlo (MC) simulations that they successfully model experimental timescales. Published KMC studies, however, deal with homogeneous substrates. The results from these simulations cannot be directly applied to diblock templates because it is not clear how to handle the borders between the PS and PMMA domains. Further, since we do not expect anisotropic diffusion within the PS or PMMA stripes [Figs. 7(a) and 7(b)] or anisotropic sticking coefficients, other phenomena must be considered as driving wire formation.

I decided to model the formation of the silver wires with a two-dimensional Monte Carlo simulation, mainly because traditional Monte Carlo simulations can accommodate all of the physical processes deduced as important from the experiments and because a qualitative comparison with experiment would be straightforward. I assumed that the metal-metal interaction dominated the metal-polymer interaction. I took the form of the metal-polymer interaction to be a difference in the mobility for silver in the PS vs the PMMA side of the diblock and a potential energy difference for the silver on the two sides of the diblock.

Before delving into details, a quick, qualitative, comparison between the simulations and experimental results can be gained by comparing Fig. 8 with Figs. 4 and 6. Results from one run of the simulation are in panels (a)–(d) of Fig. 8. The black squares represent clusters of silver atoms. The light gray background represents the PMMA side of the diblock and the dark gray background the PS. The simulation is meant to represent one 50×50 nm section of the sample. Figure 8(a) represents simulation results for low coverage and should be compared with Fig. 4(b). Figure 8(b) represents simulation results for high coverage (after evaporation of silver, but before a subsequent second anneal) and should be compared with Fig. 4(a). Finally, Fig. 8(d) represents simulation results for times after the second anneal (compare with Fig. 6).

1. Details of MC simulations

The simulations ran on a two-dimensional, 16×16 site, Cartesian lattice with periodic boundary conditions. The lattice was divided into a fast side (high mobility for the walkers) and a slow side (lower mobility for the walkers). In order to approximate the way that the atoms land on the diblock template during the experiment and the time that small clusters take to form on the substrate, the simulation

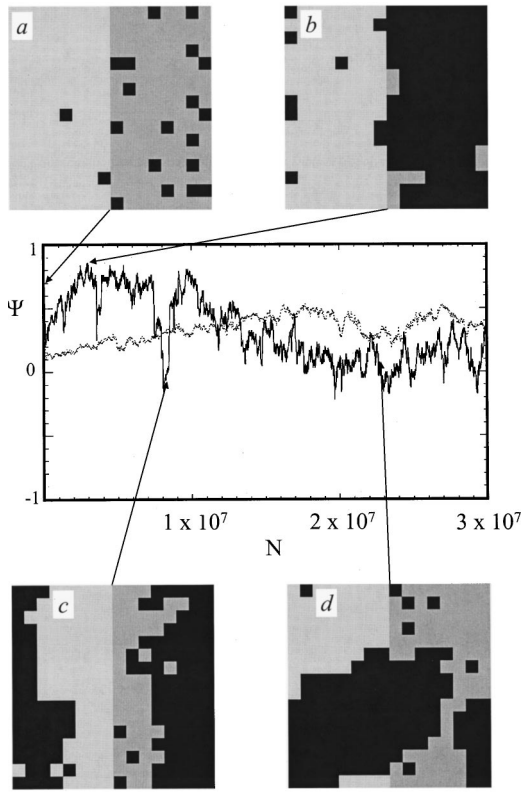

FIG. 8. Time trace of the order parameter Ψ. The graph shows a particular run of the simulation (solid line) and the average for 12 runs of the simulation (dotted line). For all runs, the simulation parameters were $m=0$ and $S=0.8$. Panels (a)–(d) show snapshots of the walkers' configuration. Each black square represents a walker. The light gray background (left side) of each panel represents the high-mobility side of the lattice and the dark gray background (right side) represents the low-mobility side of the lattice. (a) After 20 walkers have been added and 20 000 time steps elapsed. (b) After 128 walkers have been added and 3×10^6 time steps elapsed. (c) After 128 walkers have been added and 8×10^6 time steps elapsed. (d) After 128 walkers have been added and 2.3×10^7 time steps elapsed.

added individual walkers gradually to lattice, up to the number of walkers that would half fill the lattice. Half filling of the lattice allowed for a quick qualitative comparison with experimental results for wire formation. Within the simulation, a single time step consisted of randomly choosing two lattice sites. If either of the sites were unoccupied, then the time step elapsed without any actions associated with the unoccupied lattice site. If a walker occupied the first lattice site, then the simulation generated a direction in which that walker attempted to move. Similarly, if the second site were part of a cluster of walkers (defined as all walkers joined by being nearest neighbors), the simulation generated a direction in which the cluster attempted to move. The simulation accepted or rejected possible moves by the individual walkers according to the following rules.

(1) The probability for walking onto an occupied site was zero.

(2) For a walker with no nearest neighbors, the probability for accepting a move depended only on the walker's position. Moves on the fast side of the lattice were accepted with probability $p_f=1$. Moves on the slow side of the lattice were accepted with probability p_s, $0\leqslant p_s\leqslant 1$. For future reference, I define $m=p_s/p_f$.

(3) For a walker with nearest neighbors, the probability of accepting a proposed move depended on a sticking coefficient, $0\leqslant S\leqslant 1$, and the change in the number of nearest neighbors on the same cluster, Δn, that the move would bring about. If $\Delta n<0$, this probability was taken to be $(1-S)^{-\Delta n}$. If $\Delta n\geqslant 0$, this probability was set to unity.

Proposed moves for clusters were accepted with a probability equal to the average m for all walkers in the cluster, $\langle m\rangle$, divided by the number of walkers in the cluster, N, squared, that is, $\langle m\rangle/N^2$.

The fast side of the lattice represents the PMMA block of the diblock and the slow side the PS. Rule number two represents the metal's interaction with the diblock. It is equivalent to a mobility difference between the two sides of the lattice for the individual walkers combined with a potential energy difference. Detailed balance gives the energy difference ΔE between the two sides of the lattice from $m=e^{-\Delta E/KT}$, where K is Boltzman's constant and T is the absolute temperature. For $m=0$, the potential energy difference between the two sides is maximal. Rule number three represents the probability for breaking metal-metal bonds with a walker's nearest neighbors. It effectively simulates a surface tension for the clusters. Similar rules have been used elsewhere in simulations of diffusion-limited aggregation [67]. Since rule (3) above does not refer to m, it implicitly codes the fact that metal-metal interactions overwhelm metal-polymer interactions [57].

There are two factors of $1/N$ in the rule governing the mobility of the clusters. The first factor of $1/N$ corrects for the fact that by choosing a point randomly on the lattice, I am N times more likely to choose a cluster than an individual walker. For a substrate with a (three-dimensional) cluster diffusing on it and a large lattice mismatch between the two, one expects that the cluster will diffuse with Brownian trajectories with a diffusion constant roughly proportional to the inverse of the area of contact between the two [63]. Therefore, I chose to model the size dependence of the mobility of the (two-dimensional) clusters as $\sim 1/N$, which accounts for the second factor of $1/N$. I have ignored evaporation because, as noted in the discussion about Fig. 4(b) and its lower inset, evaporation does not seem to have a pronounced effect on the formation of the wires. Also, since these simulations were done on a lattice, I was unable to study any effects that the spread of a preferred crystal orientation of the silver nanostructures might have on the subsequent break up of the wire state.

2. Results from MC simulations

By comparing Figs. 8(a), 8(b), and 8(d) with Figs. 4 and 6, one can see that the above set of rules reproduces the qualitative features of both the formation and the breakup of the silver wires. This particular run of the simulation used the parameters $m=0.0$ and $S=0.8$. Figure 8(a) represents the state of the simulation after 20 000 time steps and 20 added

walkers. Almost all of the walkers have segregated to the slow side of the lattice. In a sample where I evaporated 25 Å of silver on the sample, similarly, almost all of the silver clusters that form have segregated to the PS side of the diblock [Fig. 4(a)]. Figure 8(b) represents the state of the simulation after I have added 128 walkers to the lattice (all walkers were added by step 127 000) and let the simulation continue to 3×10^6 time steps. At this point, all but one of the walkers have bonded together to form a wirelike structure (periodic boundary conditions imply that the walkers on the extreme left-hand side are actually bonded to the walkers on the right-hand side). For comparison, Fig. 4(b) shows the state of a sample after I evaporated 120 Å of silver to form nanowires. If I let the simulation progress to 2.3×10^7 time steps without additional walkers [Fig. 8(d)], the wire in the simulation breaks apart and ''balls up,'' similar to the experimental result obtained for samples with 120 Å of silver annealed for 3 h at 90 °C (Fig. 6).

I can describe the degree of wire formation by an order parameter, $\Psi=2f-1$, where f is the fraction of walkers on the slow side of the lattice. Ψ assumes values from -1 to 1 to indicate anticorrelations: when the majority of the walkers are on the fast side of the lattice, Ψ becomes negative. Figure 8 shows the evolution of Ψ as a function of the number of time steps N for a typical run of the simulation. I chose this particular run for Fig. 8 because it shows characteristics generic to the simulation in a way that makes them easy to distinguish. Empirically, I found that for 128 walkers (corresponding to half filling), $|\Psi|$ approximately equal to 0.6 or higher guarantees a continuous, wirelike path of walkers from the top to the bottom of the lattice. Long, slow changes in the order parameter, like the ones from approximately $N=1\times10^5$ to $N=3\times10^6$ or from approximately $N=1\times10^7$ to $N=2\times10^7$, correspond to shape changes of a large connected cluster of walkers. For example, the change from approximately $N=1\times10^7$ to $N=2\times10^7$ corresponds to the change from a wirelike state, shown in Figs. 8(b) or 8(c) to the ''blob'' shown in Fig. 8(d). Fast, large changes of the order parameter, like the ones around $N=8\times10^6$, correspond to translation of a wire from left to right, rather than a shape change. Compare, for example, Figs. 8(b) and 8(c). The difference is that the wire has moved a few steps to the right and, because of the periodic boundary conditions, much of the wire reappears on the left-hand side of the lattice. For very early times ($<5\times10^5$ time steps), before all of the walkers have been added to the simulation, the order parameter fluctuates near unity [Fig. 8(a)]. For $5\times10^5<N<2\times10^6$, I observe a large dip in Ψ; this dip, however, does not correspond to experimentally observed features.

For all runs of the simulation with at least 10^8 time steps, the characteristics of the order parameter pointed out here are generic: wires form and then break up, the order parameter changes quickly when a wire has stepped slightly off the slow side of the lattice, and there is some slow relaxation from a wirelike to a bloblike state. These shape changes and wire translations do not always happen at the same time. Therefore, the average order parameter, computed from an ensemble of 12 runs, slowly rises to a positive mean and fluctuates around that value (dotted line in Fig. 8).

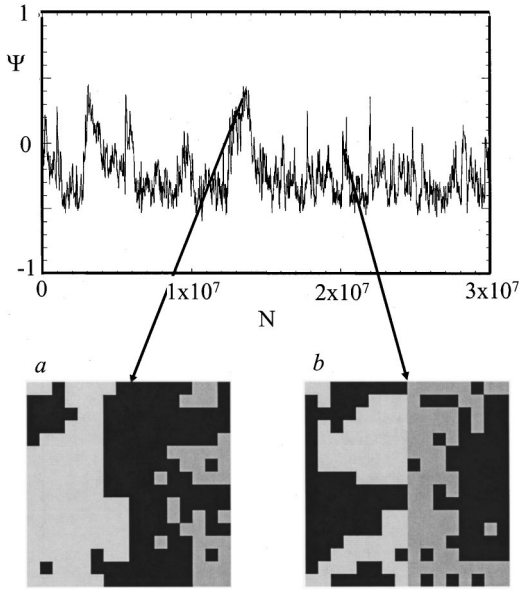

FIG. 9. Time trace of Ψ for a simulation without the energetic barrier. (a) Wirelike formation at the position of the highest order parameter value. (b) State when $\Psi\sim0$.

3. Kinetics vs energetics

In a second set of simulations, I removed the energy difference between the two sides of the diblock. This allowed me to explore the extent to which I can explain the experimental effects from kinetics alone. Detailed balance then requires that individual walkers have the same probability for taking a step from lattice site a to lattice site b as for a step from b to a. This holds for all choices of a and b and, in particular, includes cases where a and b lie on the fast and slow sides of the lattice, respectively. Further, detailed balance requires that the probability for a cluster to take a step in one direction is the same for that cluster to make the reverse trip. I find that, although wirelike structures form [Fig. 9(a)], the order parameter never exceeds 0.5. Further, relaxation into a nonwire state [Fig. 9(b)] does not take nearly as long as in simulations with an energy difference. The observed decrease in the maximum value of the order parameter implies that the relatively small (compared to the metal-metal interaction) energy difference between the slow and fast polymer regions is a key element in the formation of the wires. This appears to be not a consequence of the particular lattice chosen. Simulations run on a triangular lattice yielded similar results. One-dimensional models in which there are no particle-particle interactions may be solved analytically in both cases to show that the order parameter is monotonic with time [68], indicating that such interactions are important for the nonmonotonic evolution of the order parameter.

4. Phase diagram

Allowing for an energetic difference, I next establish the range of the parameters S and m over which the model leads to wires. For $m\rightarrow1.0$, $S=0.0$, there are no interactions between the walkers and the substrate. In this limit, the only

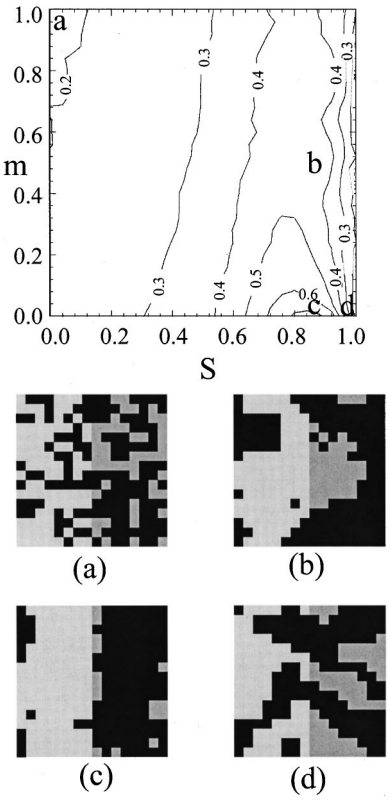

FIG. 10. Nonequilibrium ''phase diagram'' of ensemble averaged highest values of Ψ. Contour lines correspond to values of $\overline{\Psi}_{\max}(m,S)$, defined as the average of the 100 000 highest values of $\Psi(m,S,t)$ from each of ten runs of the simulation. Panels (a)–(d) show snapshots of the state when the simulation obtains the highest value of $\Psi(m,S,t)$. (a) $m=1.0$ and $S=0.0$. (b) $m=0.5$ and $S=0.8$. (c) $m=0.0$ and $S=0.84$. (d) $m=0.0$ and $S=1.0$.

interaction between the walkers themselves is a hardcore repulsion. The walkers, then, form a gas and never attain a wirelike state. For $m=0.0$, $S=0.8$, on the other hand, the walkers condense into the wirelike state discussed above. In order to best quantify the degree of wire formation for given values S and m, I calculate $\overline{\Psi}_{\max}=\langle\Psi(t)\rangle$ where the brackets correspond to averaging the 100 000 highest values of the order parameter from each of ten runs of the simulation [1 000 000 values of $\Psi(t)$ in all]. The value of $\overline{\Psi}_{\max}(m,S)$ defines a nonequilibrium phase space (Fig. 10). Figures 10(a) through 10(d) show corresponding snapshots of the walkers. I find gaseous states for $m=1$, $S=0$ [Fig. 10(a)]. The gas has a slightly higher density in the slow side of the lattice because the situation pictured corresponds to the highest value of the order parameter for that run. Simulations for which $S=1.0$, such as that shown in Fig. 10(d), do not form wires because the high sticking coefficient locks the walkers into low order parameter states that span the lattice long before the wires have a chance to form. For any walker, a sticking coefficient of one makes it impossible to decrease the number of its nearest neighbors. In particular, this prevents walkers from moving around corners on a cluster. Twenty-five spot checks along the ridge centered on the value $S=0.8$ unanimously produced structures that were continuous from the top of the lattice to the bottom; however, the vast majority of these structures had a low order parameter as Fig. 10(b) demonstrates. The highest value of $\overline{\Psi}_{\max}$ occurred for $m=0$, $S=0.84$ [Fig. 10(c)]. The state of the simulation for these parameters corresponds to a well-formed wire. Inspection of the phase space implies that the formation of high order parameter wires requires a value of m near zero and a value of S between $\sim$0.72 and $\sim$0.92.

5. Quantitative comparison with experiment

Beyond the excellent qualitative agreement, a quantitative comparison with experiment would require an experimental determination of m. I am unable, however, to directly measure the energy difference for silver on the PS vs PMMA sides of the diblock. I am also unaware of any theories, e.g., for thin film growth, that include both cluster motion and evaporation that would allow us to estimate m. The fact that almost all of the silver moves off the PMMA-domains suggests that the ratio of the diffusion constants of silver on PS and silver on PMMA is quite small. From simulations modeling situations in which (a) atoms are deposited on a substrate at random, (b) only isolated atoms are mobile, (c) the substrate is free of defects, and (d) growth of three-dimensional clusters is irreversible, Jensen *et al.* [50] find that the maximum number density of particles N^* is proportional to $(F/D)^{\alpha}$, where F is the flux of atoms incident on the substrate, D is the diffusion constant, and $\alpha=2/7$. If, instead, (b) and (d) are changed such that clusters of atoms are mobile but growth happens in two dimensions, $\alpha=0.42$ [63]. Assuming that it is appropriate to neglect evaporation and that the appropriate value of α is somewhere between these two cases, I approximate the ratio of diffusion constants of silver on PS and PMMA to be $D_{\rm PS}/D_{\rm PMMA}=(N^*_{\rm PS}/N^*_{\rm PMMA})^{1/\alpha}$, where $N^*_{\rm PS}/N^*_{\rm PMMA}$ is the ratio of the peak number densities of silver particles. I estimate m to be given by the ratio of the diffusion constants, $m\sim D_{\rm PS}/D_{\rm PMMA}=(N^*_{\rm PS}/N^*_{\rm PMMA})^{1/\alpha}$. Using the data in Fig. 7(e) to find the peak number densities, I obtain $N^*_{\rm PS}=18\times10^{-3}$ and $N^*_{\rm PMMA}=4\times10^{-3}$, and thus, $0.005<m<0.03$. This corresponds very well with the simulation result of a very large mobility contrast, $m\ll1$, for wire formation.

To estimate the relevant value for the sticking coefficient S consider the metallic bond energies. Since $1-S$ represents the probability that a walker will break an silver-silver bond, $S=1-e^{-E_b/KT}$, where E_b is the energy of the bond, K is Boltzman's constant, and T is the absolute temperature. The bond energy of diatomic silver is (160.3 ± 3.4) kJ/mol [69]. Taking this energy to approximate the bond energy on the surface of the silver particles, $S\sim1.0$. As mentioned earlier, wires do not form in the simulation for $S=1.0$ because lattice effects prohibits motion around corners when $S=1$. Thus, the model qualitatively reproduces experimental results in the correct general area of phase space.

While considering Fig. 4(b) and its lower inset at the beginning of Sec. IV, I concluded that, because changing the flux of the incoming silver did not qualitatively effect whether or not wires formed, evaporation did not significantly affect wire formation. Although evaporation is not sig-

nificant in the silver nanowire self-assembly, I expect that adding differential evaporation rates to the model, at the rates seen in the experiment, would slightly increase the area of phase space where wires form. If the evaporation rate on the fast side of the lattice were high enough, the structures that span the width of the lattice and keep wires from forming when $S=1$ would not exist. I would also have to increase the total number of walkers that were deposited on the lattice. In the extreme case, where evaporation dominates the formation of wires, the evaporation happens more rapidly than silver is deposited on the PMMA, and the only area with silver on it is the PS, where a wire then forms.

V. CONCLUSIONS, SUMMARY, AND OUTLOOK

The main thrust of this research has been to understand the self-assembly of metallic nanostructures on a PS-*b*-PMMA diblock copolymer template. Procedurally, I created my samples with a two-step self-assembly process (Fig. 1). During the first stage of self-assembly, I phase separated an ultrathin diblock copolymer film such that the surface of the film was patterned with the chemically distinct blocks forming 25 nm wide stripes [Figs. 1(a), 1(b), and 2]. During the second stage of self-assembly, I decorated this template with thermally evaporated metal [Figs. 1(c) and 1(d)] and completed the selective decoration, if necessary, by annealing the samples for a second time in an argon atmosphere. The technological advantage that this two-stage self-assembly technique has over one-stage self-assembly techniques is that the patterns created in the second stage are not dictated by the symmetries of the objects self-assembled during the second stage.

I observed two behaviors of the evaporated metals on the diblock copolymer template depending on which metals I used to decorate the film: gold, silver, bismuth, indium, lead, and tin selectively decorated the template to form arrays of nanoparticles (Fig. 3); thick (>100 Å) silver films selectively decorated the diblock template to form arrays of nanowires (Figs. 4 and 5). Most metals decorate the template with discontinuous arrays of nanoparticles because the metal's surface tension dictates that the equilibrium shape for the metal would be close to a spherical shape. The same argument, however, suggests that silver's equilibrium state is also a sphere, which raised the question of why silver forms wires. I found clues about the physical processes that take place during wire formation.

(1) Upon evaporation, atoms diffuse to form nanoclusters on top of the diblock copolymer template [Figs. 3(a) and 4(a)] [46].

(2) These clusters further diffuse on the diblock template to form larger structures with the addition of heat (Fig. 3) [25] or without it (Figs. 4 and 5).

(3) Silver diffuses along the surface of the wirelike structures that form as demonstrated by the fact that self-assembled structures have relatively smooth borders and are not fractal (Figs. 4 to 7).

(4) The silver wires are nonequilibrium structures since they relax into bulbous shapes after being even moderately heated to temperatures well below the important equilibrium temperatures for the system [Figs. 4(b) and 6].

(5) Neither the formation of the silver nanowires nor their relaxation affects the diblock template (Fig. 6).

(6) Silver diffusion and evaporation rates differ for the two materials that comprise the diblock (Fig. 7), but the evaporation rate does not qualitatively affect the formation of the nanowires [lower inset, Fig. 4(b)].

I am unaware of any theories that predict the formation of nanowires that are consistent with the experimental facts listed above. However, I show that a two-dimensional Monte Carlo simulation can qualitatively reproduce the formation of the nanowires as well as their break up (Figs. 4, 6, and 8). My Monte Carlo simulation runs on a 16×16 lattice with periodic boundary conditions. High- and low-mobility halves of the lattice, with mobility ratio m, represent the interaction of the silver with the PMMA and PS blocks. I model the particle-particle interactions as a hardcore repulsion and an attractive interaction mediated by a sticking coefficient S. The cluster mobility is taken to vary as $1/N$, where N is the number of walkers in a cluster. I include an energy difference (small in comparison to the silver-silver interaction) to take into account the slightly more favorable silver-PS interaction (as compared to silver PMMA). Without either this energy difference (Figs. 8 and 9) or the cluster mobility (not shown here), we did not find qualitative agreement with the experimental results.

For several reasons, the amount of agreement between the experiment and the simulation is remarkable. The present simulation runs in two dimensions even though the wires form in three dimensions (Fig. 5). The simulation does not include the effects of physical processes that I expect have a minor influence on the wire formation: evaporation of silver from the diblock template and how the spread of regions of constant crystallization affects how quickly the wires relax. The latter may explain why the silver nanowires relax so slowly [70]. My model assumes knowledge of metallic interaction with polymer systems, which, at the moment, is underdeveloped despite its relevance to industrial concerns (e.g., photolithography). In particular, we need increased study into metallic diffusion in polymers and diblocks, and knowledge of differential energies of metals in either block of a diblock.

A more quantitative comparison with experiment may require a more realistic model. The present simulation, however, clearly points out the possibility of tailoring systems (diblock template+metal) such that wire formation might be optimized. The parameter S, which measures the cohesive energy of the metal, is out of experimental control for single elements; but the parameter m may be changed by a judicious choice of polymer and metal. A polymer containing a chemical group known to have a strong interaction with a ferromagnet, for instance, would yield magnetic wires. Further, the patterns generated in the wires could be controlled with an electric field to yield nontrivial patterns [71–73]. As an immediate application of the arrays of nanoparticles and nanowires, I have studied the transport properties of these arrays. These results have been published elsewhere [47].

ACKNOWLEDGMENTS

It is my pleasure to acknowledge many thought provoking and stimulating discussions on this topic with Heinrich Jaeger, Tom Witten, Susan Coppersmith, and David Grier. I would like to also thank both Rebecca Jackson and Heinrich Jaeger for critically reading the manuscript and P. Infante of the Cornell Nanofabrication Facility for assistance with creating the Si_3N_4 membrane substrates. I am also deeply indebted to Terry Morkved for showing me his investigations into metal decoration of diblock copolymers. This research has been supported by the MRSEC program of the National Science Foundation under Grant No. DMR-9808595 and by the Keck Foundation under Grant No. 991705.

[1] R. Williams and R. S. Crandall, Phys. Lett. **48A**, 225 (1974).
[2] R. Williams, R. S. Crandall, and P. J. Wojtowicz, Phys. Rev. Lett. **37**, 348 (1976).
[3] N. A. Clark, A. J. Hurd, and B. J. Ackerson, Nature (London) **281**, 57 (1979).
[4] D. J. W. Aastuen, N. A. Clark, L. K. Cotter, and B. J. Ackerson, Phys. Rev. Lett. **57**, 1733 (1986).
[5] C. P. Collier, R. J. Sakally, J. J. Shiang, S. E. Henrichs, and J. R. Heath, Science **277**, 1978 (1997).
[6] F. S. Bates and G. H. Fredrickson, Annu. Rev. Phys. Chem. **41**, 525 (1990).
[7] F. S. Bates and G. H. Fredrickson, Phys. Today **52** (2), 32 (1999).
[8] M. Mundschau, E. Bauer, and W. Swiech, J. Appl. Phys. **65**, 581 (1989).
[9] T. Jung, R. Schlittler, J. K. Gimzewski, and F. J. Himpsel, Appl. Phys. A: Mater. Sci. Process. **61**, 467 (1995).
[10] D. Y. Petrovykh, F. J. Himpsel, and T. Jung, Surf. Sci. **407**, 189 (1998).
[11] M. Paunov and E. Bauer, Appl. Phys. A: Solids Surf. **A44**, 210 (1987).
[12] J. Viernow, D. Y. Petrovykh, F. K. Men, A. Kirakosian, J.-L. Lin, and F. J. Himpsel, Appl. Phys. Lett. **74**, 2125 (1999).
[13] J. de la Figuera, M. A. Huerta-Garnica, J. E. Prieto, C. Ocal, and R. Miranda, Appl. Phys. Lett. **66**, 1006 (1995).
[14] F. J. Himpsel, T. Jung, Al Kirakosian, J.-L. Lin, D. Y. Petrovykh, H. Rauscher, and J. Viernow, MRS Bull. **24**, 20 (1999).
[15] F. J. Himpsel, Y.-W. Mo, T. Jung, J. E. Ortega, G. J. Mankey, and R. F. Willis, Superlattices Microstruct. **15**, 237 (1994).
[16] R. Nötzel, N. N. Ledentsov, L. Däwertz, M. Hohenstein, and K. Ploog, Phys. Rev. Lett. **67**, 3812 (1991).
[17] R. Saito, S. I. Okamura, and K. Ishizu, Polymer **33**, 1099 (1992).
[18] Y. N. C. Chan and R. R. Schrock, Chem. Mater. **4**, 24 (1992).
[19] Y. N. C. Chan, R. R. Schrock, and R. E. Cohen, J. Am. Chem. Soc. **114**, 7295 (1992).
[20] Y. N. C. Chan, G. S. W. Craig, R. R. Schrock, and R. E. Cohen, Chem. Mater. **4**, 885 (1992).
[21] C. C. Cummins, R. R. Schrock, and R. E. Cohen, Chem. Mater. **4**, 27 (1992).
[22] D. E. Fogg, L. H. Radzilowski, R. Blanski, R. R. Schrock, and E. L. Thomas, Macromolecules **30**, 417 (1997).
[23] V. Sankaran, C. C. Cummins, R. R. Schrock, R. E. Cohen, and R. J. Silbey, J. Am. Chem. Soc. **112**, 6858 (1990).
[24] R. Tassoni and R. R. Schrock, Chem. Mater. **6**, 744 (1994).
[25] T. L. Morkved, P. Wiltzius, H. M. Jaeger, D. G. Grier, and T. A. Witten, Appl. Phys. Lett. **64**, 422 (1994).
[26] R. W. Zehner, W. A. Lopes, T. L. Morkved, H. M. Jaeger, and L. R. Sita, Langmuir **14**, 241 (1998).
[27] R. W. Zehner and L. R. Sita, Langmuir **15**, 6139 (1999).
[28] T. Hashimoto, K. Txutsumi, and Y. Funaki, Langmuir **13**, 6869 (1997).
[29] T. Thurn-Albrecht, J. Schotter, G. A. Kästle, N. Emley, T. Shibauchi, L. Krusin-Elbaum, K. Guarini, C. T. Black, M. T. Tuominen, and T. P. Russell, Science **290**, 2126 (2001).
[30] M. Park, C. Harrison, P. M. Chaikin, R. A. Register, and D. H. Adamson, Science **276**, 1401 (1997).
[31] C. Harrison, M. Park, P. M. Chaikin, R. A. Register, and D. H. Adamson, J. Vac. Sci. Technol. B **16**, 544 (1998).
[32] J. P. Spatz, T. Herzog, S. Mößmer, P. Ziemann, and M. Möller, Adv. Mater. **11**, 149 (1999).
[33] P. Lambooy, T. P. Russell, G. J. Kellogg, A. M. Mayes, P. D. Gallagher, and S. K. Satija, Phys. Rev. Lett. **72**, 2899 (1994).
[34] G. J. Kellogg, D. G. Walton, A. M. Mayes, P. Lambooy, T. P. Russell, P. D. Gallagher, and S. K. Satija, Phys. Rev. Lett. **76**, 2503 (1996).
[35] N. Koneripalli, R. Levicky, F. S. Bates, J. Ankner, H. Kaiser, and S. K. Satija, Langmuir **12**, 6681 (1996).
[36] N. Koneripalli, N. Singh, R. Levicky, F. S. Bates, P. D. Gallagher, and S. K. Satija, Macromolecules **28**, 2897 (1995).
[37] T. L. Morkved and H. M. Jaeger, Europhys. Lett. **40**, 643 (1997).
[38] T. L. Morkved, Ph.D. thesis, The University of Chicago, 1997.
[39] W. H. Tang and T. A. Witten, Macromolecules **31**, 3130 (1998).
[40] J. Hahm, W. A. Lopes, H. M. Jaeger, and S. J. Sibener, J. Chem. Phys. **109**, 10 111 (1998).
[41] C. Harrison, D. H. Adamson, Z. Cheng, J. M. Sebastian, S. Sethuraman, D. A. Huse, R. A. Register, and P. M. Chaikin, Science **290**, 1558 (2000).
[42] I have also observed a third mode, which I will not report on here, where the evaporated metal does not respect the underlying template at all and forms a sheet over the diblock surface.
[43] T. L. Morkved, W. A. Lopes, J. Hahm, S. J. Sibener, and H. M. Jaeger, Polymer **39**, 3871 (1998).
[44] E. L. Thomas and Y. Talmon, Polymer **19**, 225 (1978).
[45] T. L. Morkved, P. Wiltzius, H. M. Jaeger, D. G. Grier, and T. A. Witten, Appl. Phys. Lett. **63**, 322 (1993) erroneously stated that gold decorated the PMMA domains.
[46] B. Lin, T. L. Morkved, M. Meron, Z. Huang, P. J. Viccaro, H. M. Jaeger, S. M. Williams, and M. L. Schlossman, J. Appl. Phys. **85**, 3180 (1999).
[47] W. A. Lopes and H. M. Jaeger, Nature (London) **414**, 735 (2001).
[48] The glass temperatures of the individual blocks are between 100 and 105 °C and, empirically, glass temperatures of

diblocks fall between the glass temperatures of the individual blocks [F. Rodriguez, *Principles of Polymer Systems* (Taylor & Francis, London, 1996)].
[49] T. Castro, R. Reifenberger, E. Choi, and R. P. Andres, Phys. Rev. B **42**, 8548 (1990).
[50] P. Jensen, H. Larralde, M. Meunier, and A. Pimpinelli, Surf. Sci. **412/413**, 458 (1998).
[51] J. R. Sambles, Proc. R. Soc. London, Ser. A **324**, 339 (1971).
[52] L. E. Murr, *Interfacial Phenomena in Metals and Alloys* (Addison-Wesley, Reading, MA, 1975).
[53] S. Wu, *Polymer Interface and Adhesion* (Marcel Dekker, New York, 1982).
[54] D. Lando, J. F. Bohland, and W. C. Hahn, J. Phys. Chem. **77**, 1969 (1973).
[55] F. Piuz and J. P. Borel, Phys. Status Solidi A **14**, 129 (1972).
[56] J. R. Sambles, L. M. Skinner, and N. D. Lisgarten, Proc. R. Soc. London, Ser. A **318**, 507 (1970).
[57] L. J. Gerenser and K. E. Goppert-Berarducci, in *Metallized Plastics 3: Fundamental and Applied Aspects*, edited by K. L. Mittal (Plenum, New York, 1992), p. 163.
[58] H. Gau, S. Herminghaus, P. Lenz, and R. Lipowsky, Science **283**, 46 (1999).
[59] P. Lenz and R. Lipowsky, Phys. Rev. Lett. **80**, 1920 (1998).
[60] S. Herminghaus, A. Fery, S. Schlagowski, K. Jacobs, R. Seemann, H. Gau, W. Mönch, and T. Pompe, J. Phys.: Condens. Matter **11**, A57 (1999).
[61] J. A. Venables, G. D. T. Spiller, and M. Hanbücken, Rep. Prog. Phys. **47**, 399 (1984).
[62] H. Brune, Surf. Sci. Rep. **31**, 121 (1998).
[63] P. Jensen, Rev. Mod. Phys. **71**, 1695 (1999), and references therein.
[64] H. Röder, E. Hahn, H. Brune, J.-P. Bucher, and K. Kern, Nature (London) **366**, 141 (1993).
[65] Y.-W. Mo, B. S. Swartzentruber, R. Kariotis, M. B. Webb, and M. G. Lagally, Phys. Rev. Lett. **63**, 2393 (1989).
[66] Y. W. Mo, J. Kleiner, M. B. Webb, and M. G. Lagally, Phys. Rev. Lett. **66**, 1998 (1991).
[67] T. A. Witten and L. M. Sander, Phys. Rev. B **27**, 5686 (1983).
[68] S. Coppersmith (private communication).
[69] J. A. Kerr, in *CRC Handbook of Chemistry and Physics 1999-2000: A Ready-Reference Book of Chemical and Physical Data*, 79th ed., edited by D. R. Lide (CRC, Boca Raton, 1998).
[70] N. Combe, P. Jensen, and A. Pimpinelli, Phys. Rev. Lett. **85**, 110 (2000).
[71] T. L. Morkved, M. Lu, A. M. Urbas, E. E. Ehrichs, H. M. Jaeger, P. Mansky, and T. P. Russel, Science **273**, 931 (1996).
[72] T. L. Morkved, W. A. Lopes, M. Lu, A. M. Urbas, H. M. Jaeger, P. Mansky, and T. P. Russel, in *Morphological Control in Multiphase Polymer Mixtures*, edited by R. M. Briber, C. C. Han, and D. G. Peiffer, Mater. Res. Soc. Symp. Proc. No. 461 (Materials Research Society, Pittsburgh, 1997), p. 109.
[73] P. Mansky, J. DeRouchey, T. P. Russell, J. Mays, M. Pitsikalis, T. L. Morkved, and H. M. Jaeger, Macromolecules **31**, 4399 (1998).